ACS Energy LETTERS

http://pubs.acs.org/journal/aelccp

LETTER

Long Period Voltage Oscillations Associated with Reaction Changes between CO_2 Reduction and H_2 Formation in Zero-Gap-Type CO_2 Electrochemical Reactor

Nagisa Mikami, Kei Morishita, Takeharu Murakami, Takuya Hosobata, Yutaka Yamagata, Takayo Ogawa, Yoshiharu Mukouyama, Shuji Nakanishi, Joel W. Ager, III,* Katsushi Fujii,* and Satoshi Wada

Cite This: *ACS Energy Lett.* 2024, 9, 4225−4232

Read Online

ACCESS | Metrics & More | Article Recommendations | Supporting Information

ABSTRACT: Zero-gap-type reactors with gas diffusion electrodes (GDE) that facilitate the CO_2 reduction reaction (CO_2RR) are attractive due to their high current density and low applied voltage. These reactors, however, suffer from salt precipitation and anolyte flooding of the cathode, leading to a short lifetime. Here, using a zero-gap reactor with a transparent cathode end plate, we report periodic voltage oscillations under constant current operation. Increases in cell voltages occur at the same time as the reactor switches from the hydrogen evolution reaction (HER) to predominant CO_2RR; decreases in cell voltage occur with the switch from the CO_2RR to HER. Further, real time visual observations show that salt precipitation occurs during the CO_2RR, whereas salt dissolution occurs during the HER. Slow flooding triggers the transition from the CO_2RR to HER. A number of processes combine to slowly reduce the water content in the microporous layer, which triggers the transition back to the CO_2RR.

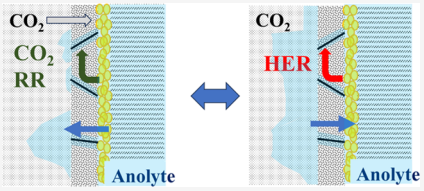

The reduction of carbon dioxide (CO_2) exhaust is an urgent problem for human beings. Electrochemical CO_2 reduction reactions (CO_2RR) to convert CO_2 into useful chemicals is an approach to solve this problem,[1,2] thus motivating its study over several decades.[3] Research on the CO_2RR has mainly focused on the control of product selectivity and reduction of the overpotential.[4,5] Due to the low solubility of CO_2 in aqueous electrolytes and the low CO_2 diffusion coefficient,[6,7] many types of reactors have also been investigated including H-type cells, gas-flow-type reactors (gas-flow-type reactors usually have flowing catholytes and anolytes and use a gas diffusion electrode such that CO_2 gas can be supplied from the backside of the cathode electrode), and zero-gap-type reactors.[8] The current density for the CO_2RR is over 1 A/cm^2 in recent reports using flow-type reactors,[1,9] but the applied voltage is still high. Anion exchange membrane (AEM) based membrane electrode assembly (MEA) zero-gap-type reactors with gas diffusion electrodes (GDEs) shown in Scheme 1a are currently believed to be the most suitable approach to lower the operating voltage.[2] Although the lifetime is relatively good when CO-producing Ag electrocatalysts are used,[10] stability remains a challenge when Cu-based electrocatalysts making multicarbon products are used.

The short lifetimes of zero-gap-type reactors with Cu electrochemical catalysts are caused by salt precipitation and electrolyte flooding of the cathode.[11−13] Both processes block access of CO_2 gas to the catalyst. Further, it has been suggested that both phenomena are caused by the electromigration of hydrated K^+ ions and electrolyte migration from the anode to the cathode.[14]

The full-cell voltage for CO_2RR of the zero-gap reactor is usually constant under constant current operations.[15,16] However, voltage oscillations have been observed in some cases, depending on the operating conditions. Analysis of the voltage oscillation phenomenon should be useful for understanding the CO_2R mechanism in zero-gap reactors. A recent study of voltage oscillation used X-ray tomography to visualize the salt precipitation and the resultant flooding in the electrode.[17,18] The relative rates of the CO_2RR and HER reactions were also associated with changes in cell potential,

Received: May 7, 2024
Revised: June 17, 2024
Accepted: July 15, 2024
Published: August 1, 2024

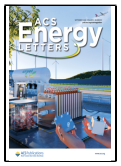

Scheme 1. (a) Schematic Structure of the Cathode Region in the Zero-Gap-Type CO_2R Reactor[a] and (b) Schematic Diagram of a Whole Zero-Gap-Type Reactor[b]

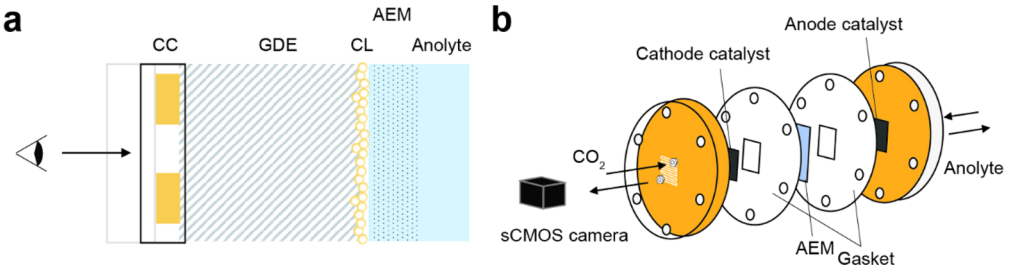

[a]Abbreviations: CC, current collector and serpentine gas flow with transparent end plate; GDE, gas diffusion electrode; CL, catalyst layer; AEM, anion exchange membrane. The anolyte is in the GDE anode. [b]A CMOS camera was utilized to track the time progression of salt precipitation in the flow field channels.

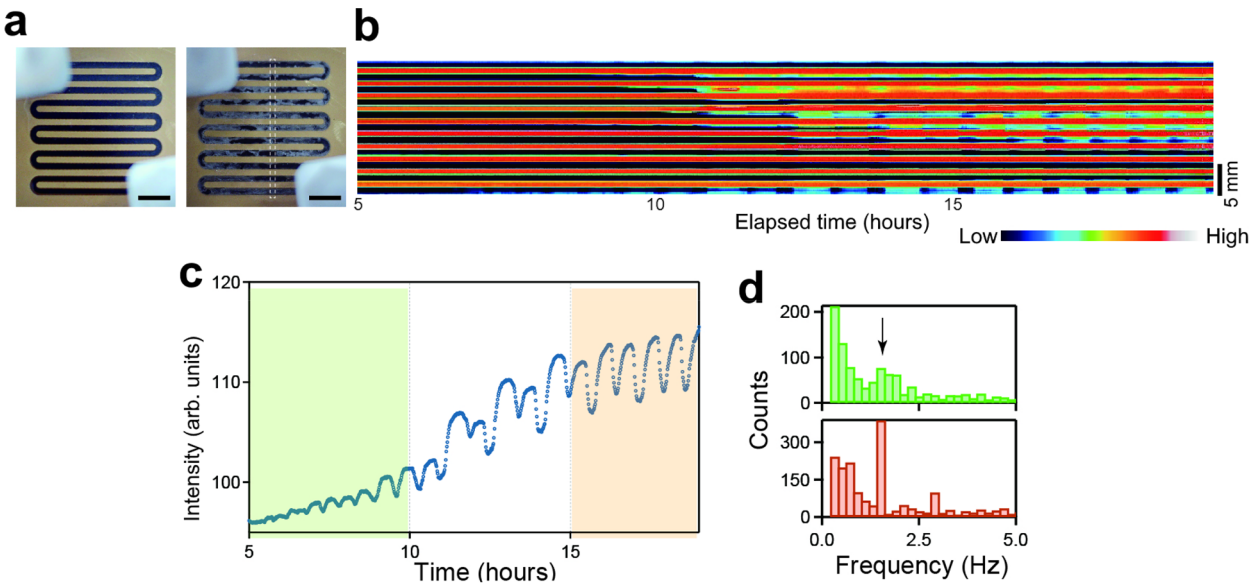

Figure 1. (a) Photographs of the cathode through the transparent end plate: (left) reactor as fabricated; (right) after 5 h of operation. The dotted rectangle denotes the region of interest (ROI) used for the kymograph in (b) and integrated intensity versus time data in (c). The kymograph, which spans from 5 h after the initiation of the experiment to 19 h, demonstrates the periodic oscillation in intensity. To clearly see the periodic oscillation in intensity, the pseudo color was applied, with the yellow and black colors representing high intensity (salt precipitation) and low intensity (electrolyte flooding with salt dissolution), respectively. (d) Frequency analysis of (c). The green (upper) and orange (lower) colors represent the frequencies at 5−10 and 15−19 h from the start of the experiment, respectively. The current density was 200 mA/cm^2 at RT using a 5 cm^2 electrode with a Sustainion membrane. The anolyte was aqueous 0.1 M $KHCO_3$. The flow rate of CO_2 was 70 mL/min.

and a model linking changes in the ion transport capacity of the membrane with cell potential was proposed. However, it was not possible to develop a more detailed mechanism like the order of the processes due to limitations of the employed observation methods.

In this study, the salt precipitation and electrolyte flooding were observed visually using a usual-sized zero-gap-type cell with transparent cathode end plate to clarify the order of the processes (Scheme 1a) with a 0.1 M $KHCO_3$ anolyte and constant current operation of 200 mA/cm^2 for a 5 cm^2 electrode area. As shown in Scheme 1b, this arrangement allows real-time observation of the cathode electrode gas-flow region from the backside. Previous studies have employed a similar approach,[19,20] but our experimental system is equipped with a CMOS camera which can track the conditions at the cathode backside in real time with data collected every 10 s to 1 min. For example, the image from the CMOS camera shown in Figure 1a clearly shows the backside of the gas diffusion electrode (GDE) of the cathode through the serpentine gas channel. To the right is an image taken after 5 h of operation; salt precipitation (white areas) on the backside of the GDE is clearly visible (Figure 1a, right).

Under long-term, constant current operation (200 mA/cm^2), periodic voltage oscillations in our MEA cell were frequently observed (Cu on Sigracet GDE, 0.1 M $KHCO_3$ anolyte; more details of operating conditions are in section S.1, Reactor structures and Experimental conditions). Image analysis establishes a clear link between the cell voltage and salt formation: salt precipitation is associated with increases in full-cell voltage, whereas salt dissolution triggers a transition to lower voltage operation (Supplementary Movie 1). This kind of oscillation phenomenon requires slow negative feedback or time-delayed negative feedback. The analyses described below will show that the electrolyte ingress into the GDE during the CO_2RR and the change in gas generation rate at the cathode

https://doi.org/10.1021/acsenergylett.4c01256
ACS Energy Lett. 2024, 9, 4225−4232

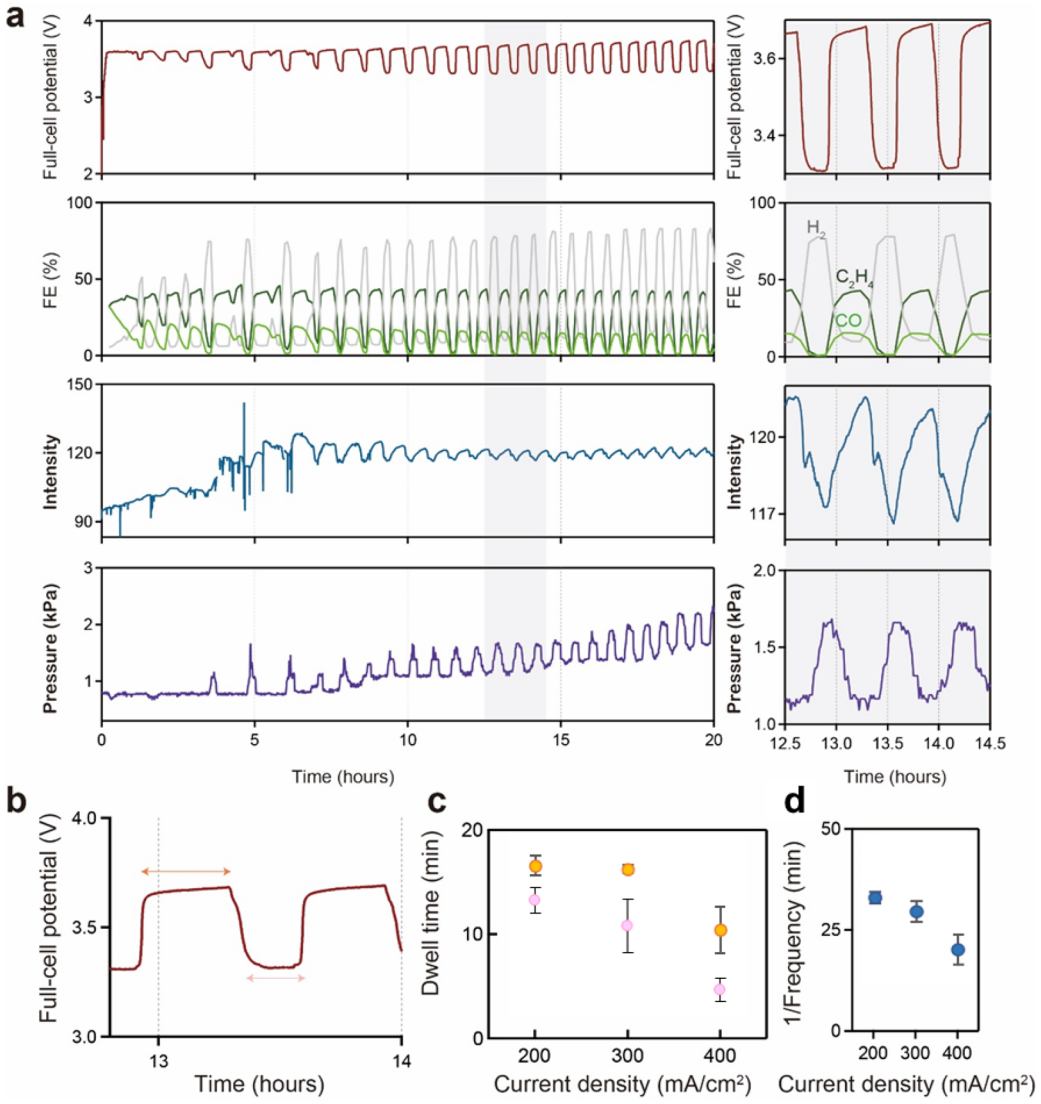

Figure 2. (a) (top) Repetitive oscillations in the reactor full-cell voltage. (upper middle) Faradaic efficiency (FE) of ethylene (C_2H_4), carbon monoxide (CO), and hydrogen (H_2), represented by dark green, light green, and gray colors, respectively. (lower middle) Intensity of the entire image of MEA. (bottom) CO_2 gas pressure in the cell. The right graphs represent magnified images of the gray area in the left graphs. Comparison between the upper and lower middle graphs reveals that high-intensity (salt precipitation) areas indicate CO_2 reduction (CO and C_2H_4 formation observed), while low-intensity areas represent HER occurrence. Furthermore, the comparison between the intensity of the image (lower middle) and the full-cell voltage (top) graph exhibits a positive correlation that the voltage decrease corresponds to a decrease in intensity (salt dissolution) while the voltage increase results in an intensity increase (salt precipitation). (b) Dwell time analysis where the time course of cell voltage was depicted, with the orange and pink arrows indicating the dwell time at high and low voltages, respectively, corresponding to the data on (c). Dwell time was defined as a duration without the voltage change. (c) Dependence of dwell time on current density (n = 5). (d) Dependence of oscillation intervals (1/frequency) on current density (n = 5). The error bars in (c) and (d) show the time between 10% low from maximum values and 10% high from minimum values for all oscillations in the condition shown. The current density was 200 mA/cm^2 at RT using a 5 cm^2 electrode with a Sustainion membrane. The anolyte was aqueous 0.1 M $KHCO_3$. The flow rate of CO_2 was 70 mL/min.

when the dominant reaction is the HER are the reasons for the voltage oscillation under constant current conditions.

Since the salt precipitation did not occur uniformly throughout the electrode, data taken from a specific area would not yield a quantitative analysis (Figure S3). Therefore, we enclosed the entire width from inlet to outlet of the serpentine-shaped flow field with the square in Figure 1a, right, and tracked the time course of its mean brightness (see section S.1, Reactor structures and Experimental conditions, and Figure 1b). By using a pseudocolor analysis of the intensity profile (kymograph), we can visualize the rates of salt precipitation and dissolution on the electrode (Figure 1c). Focusing on the local area, the salt precipitation and dissolution start from the edge of the metal electrode (Figure S4).

Via Fourier analysis, the oscillation period in the first 5−10 h of small-amplitude oscillation is about 40 min (Figure 1d, green), and it continues during 15−20 h of operation with increasing amplitude (Figure 1d, orange). Similar periodic oscillations were repeatably observed under the same experimental conditions (Figure S5). The voltage oscillation phenomenon was also observed when a metal end plate (not transparent) was used (Figure S6). This shows that the

https://doi.org/10.1021/acsenergylett.4c01256
ACS Energy Lett. 2024, 9, 4225−4232

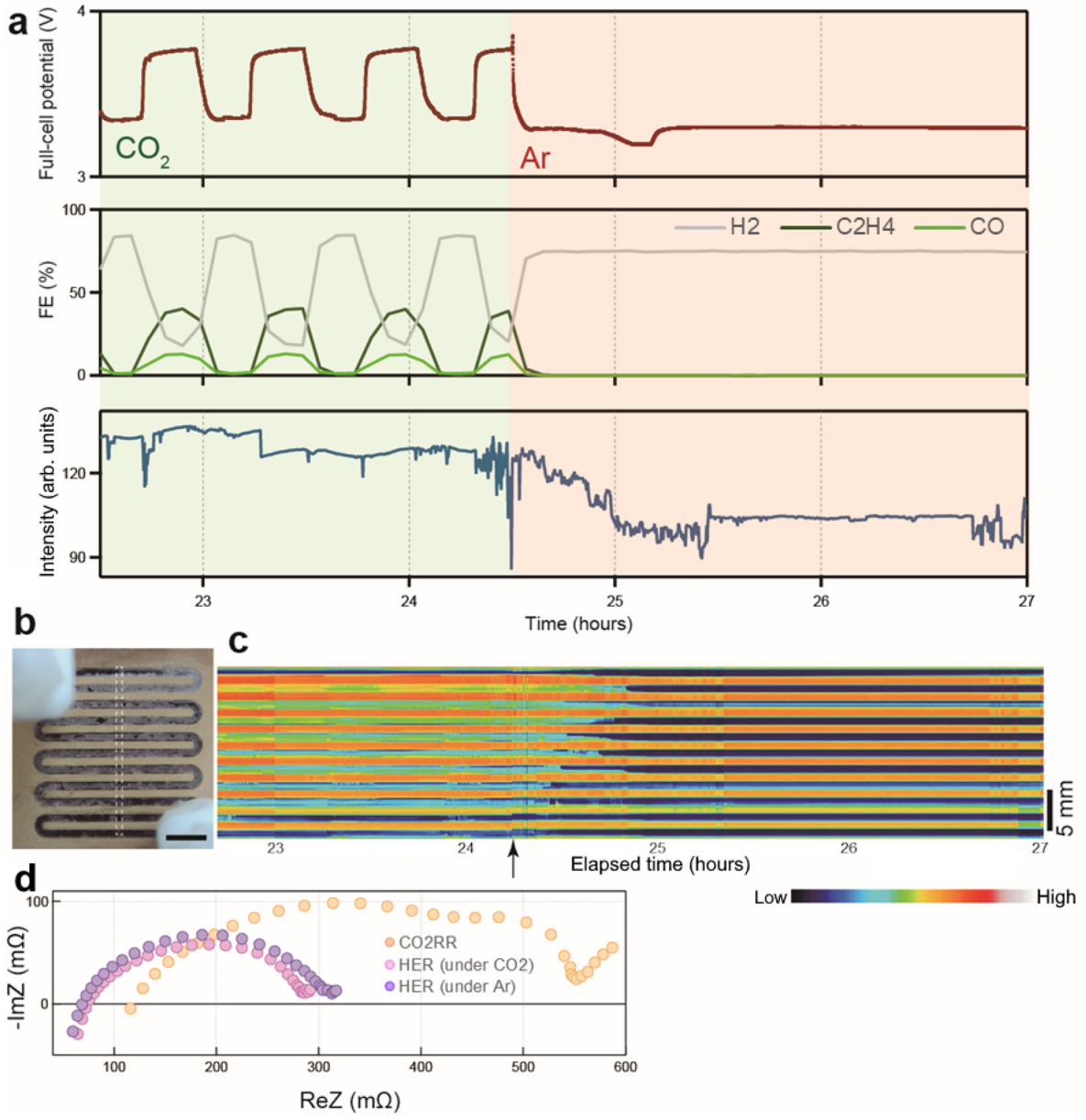

Figure 3. (a) Full-cell voltage (top), Faradaic efficiency (FE, middle) of ethylene (C_2H_4), carbon monoxide (CO), and hydrogen (H_2), represented by dark green, light green, and gray colors, respectively, and the intensity of the entire image of MEA (bottom). After 24.5 h, the background color changed from green to orange, indicating the switching from CO_2 to Ar supply to the cathode. The maximum FE under Ar supply conditions is lower than the real value because of the viscosity correction of base gas being used for CO_2. (b) Photograph of an MEA, with the chosen location for the kymograph (c) creation marked by a dotted rectangle. (c) Kymograph displaying the last 4.5 h of the 27 h experiment. A pseudocolor was applied, with black and white indicating high and low intensity, respectively. The arrow indicates the time at which CO_2 was switched to Ar. (d) Impedance measurement with the colors being represented by orange, pink, and purple lines, which correspond to high voltage (CO_2RR), low voltage (HER) during CO_2 supply, and replacement from CO_2 to Ar, respectively. ReZ and ImZ indicate the real and imaginary components of the impedance, respectively. The oscillating amplitude was 40 mA (8 mA/cm^2) from 100 kHz to 1 Hz at a current of 1000 mA (200 mA/cm^2). The current density was 200 mA/cm^2 at RT for the 5 cm^2 electrode with the Sustainion membrane. The anolyte was a 0.1 M $KHCO_3$ aqueous solution. The flow rate of CO_2 was 70 mL/min.

fluctuations are independent of the material used for the cathode plate.

To further characterize the oscillations in salt precipitation/dissolution and the voltage, we compared the Faradaic efficiency of the cathode products of C_2H_4, CO, and H_2 with the intensity of the GDE image (Figure 2a). Although the products of the CO_2RR were mainly C_2H_4, CH_4, CO, and H_2 in the gas phase and alcohols and aldehydes in the liquid phase, here the focus was on major gas phase products C_2H_4 and CO. High- and low-voltage operation corresponds to predominant CO_2RR and HER, respectively (Figure 2a, top and upper middle). Further, high/low full-cell voltages correspond to high intensity of the image (salt precipitation) and low intensity of the image, respectively (Figure 2a, top and lower middle).

The period of the voltage oscillation becomes shorter with increasing current density from 100 to 400 mA/cm^2 (Figure S7). To quantitatively analyze this phenomenon, we estimated

https://doi.org/10.1021/acsenergylett.4c01256
ACS Energy Lett. 2024, 9, 4225−4232

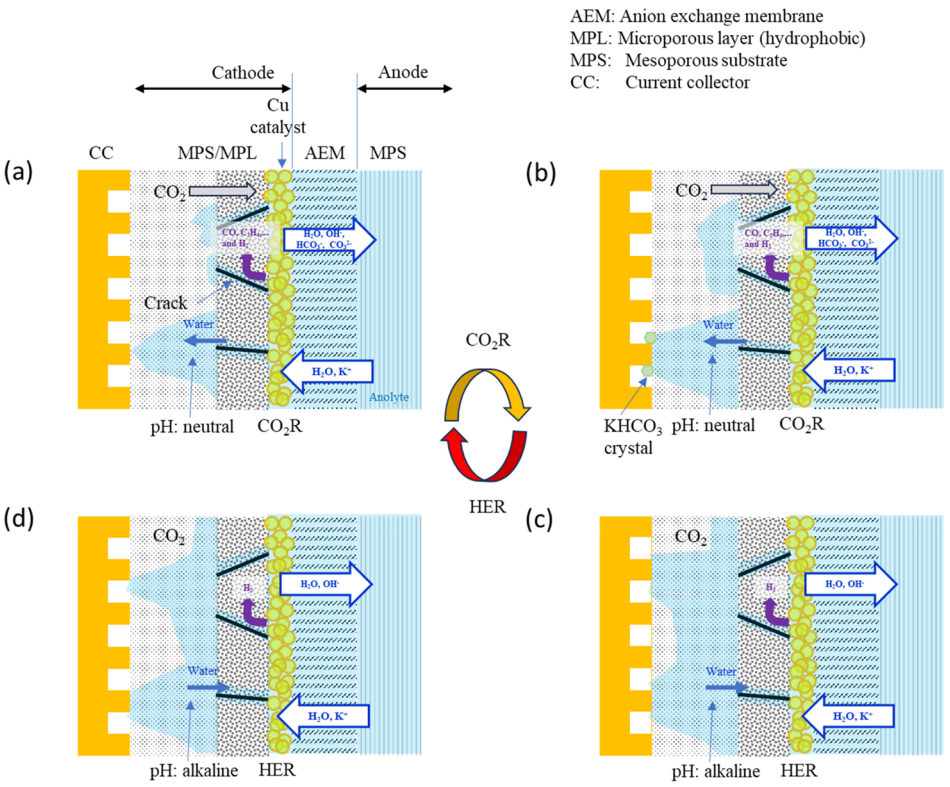

Figure 4. Schematic depiction of the model for the voltage oscillation. A detailed description of states (a−d) and of the transitions between them are given in the main text.

the dwell time (Figure 2b) of the CO_2RR (dCO_2RR: Figure 2c, pink) and the dwell time of the HER (dHER: Figure 2c, orange), corresponding to the duration of high-voltage and low-voltage regions, respectively. dCO_2RR and dHER became shorter with increasing current density. The period of salt precipitation/dissolution was consequently decreased as well (Figure 2d).

To investigate whether the oscillations were specific to constant current operation, we changed the operation mode from constant current (200 mA/cm^2) to constant voltage (3.5 and 3.7 V). In this mode, periodic oscillations in cell current were observed whose frequency increased with voltage (Figure S8). Clearly, the oscillations are not associated with the way the electrolysis cell is powered.

To evaluate the CO_2 gas effect, we switched the injection gas from CO_2 to Ar (with 200 mA/cm^2 constant current) under conditions with partial salt precipitation in the channels. After 4−10 min later, the salt dissolved into the electrolyte. The electrolyte accumulated partially at the top of the metal electrode plate (bottom-side of the CO_2 gas pathway) after 20 min. The electrolyte disappeared after 30 min, at which point the salt was pushed out of the cell. After that, salt precipitation and flooding were not observed (Supplementary Movie 2 and Figure S9).

As a result, the periodic voltage oscillations stopped and the voltage stayed in the low-voltage state, which is the signature of the HER (Figure 3a, top and middle). Furthermore, all the observable salt precipitation disappeared (Figure 3a, bottom, and Figure 3b,c). We observed the electrode for 150 min after the gas was switched from CO_2 to Ar but did not see any further salt precipitation (see also Supplementary Movie 3). When the gas supply was returned from Ar to CO_2, the voltage increased rapidly, and the voltage oscillation started again (Figure S10). The full-cell voltage is higher under CO_2 supply than with Ar at the same current density (e.g., ∼3.7 V vs ∼3.3 V at 200 mA/cm^2; see Figure S11). From this, we infer that the lowest overpotential HER sites are occupied, probably by CO, during the CO_2RR.

We performed impedance measurements to investigate the resistance losses in the cell.[21] Galvanic electrochemical impedance spectroscopy (GEIS) under current control shows the resistance of the membrane (x-intercept of the semicircle) and the other resistance (diameter of the semicircle) by the overpotentials due to electrode−electrolyte interfaces and the pH difference between the anode and cathode in the entire reactor (Figure 3d). Although the impedance spectrum for the high voltage (orange, t = 22.73 h) is different from the low voltage in CO_2 supply (pink, t = 24.69 h), the spectrum for the low voltage coincided with that measured with Ar supply (purple, t = 27.40 h) in Figure 3d. This indicates that the HER in CO_2 supply was the same condition in Ar supply, that is, the CO_2 gas was not appropriately supplied to the catalytic region. The series resistances were also different in the cases of high and low voltages. This probably indicates that the resistivity of the electrolyte in the cathode and/or the AEM changes; that is, the low resistivity is expected in the low-voltage period of the HER.

At this point, we suspected that the oscillations were associated with liquid electrolyte ingress into the GDE. We found that the oscillation period increased when the CO_2 pressure in the cell was reduced (Figure S12). The oscillations persisted but became aperiodic when the pressure of the anode side was increased by using a clamp to restrict the anolyte circulation (Figure S13). The electrolyte concentration and the current density may also affect the electrolyte migration speed and direction from the migration model experiments (see

https://doi.org/10.1021/acsenergylett.4c01256
ACS Energy Lett. 2024, 9, 4225−4232

section S.3, Electrolyte migration dependence on the pressure between the anode and the cathode, and Figures S14−S16).

In the model, we propose that changes in the electrolyte volume in the GDE cause the oscillatory CO_2RR and HER behavior in our MEA cell (Figure 4; see also section S.4 ,Voltage oscillation analysis, and Supplementary Movie 3). This clearly shows that the complete electrolyte covering of the cathodic catalyst causes the CO_2RR to change to the HER, and the partial CO_2 supply recovery to the cathodic catalyst causes the change from the HER to the CO_2RR. That is, the physical conditions of the electrolyte and the cathodic catalyst are probably the reason for the reaction changes. This means that the order of the voltage oscillation process is different from the previous model.[18] That is, the electrolyte flooding at the cathode occurs before the HER, and not the water flux to the cathode increasing after the HER starts.

The oscillations between the HER and CO_2RR are comparable to those reported by Seger and co-workers for similarly constructed AEM-based electrolysis cells.[18,22] The remarkable periodicity of the oscillations observed here is evident in Figure 2a and is emphasized in the phase portrait shown in Figure S17 (Supplementary Movie 4). Clearly, the system is bistable and supports a mechanism which can trigger the transition between the two metastable states. However, this bistable phenomenon will not continue indefinitely, because the periodic salt precipitation and dissolution will differ in position and amount for each cycle. Still, since these bistable phenomena clarify each condition, especially the electrolyte existence in the cathode for the CO_2RR and HER; the analysis of these states is useful to obtain the guidelines of the stable CO_2RR. Oscillations of either current or potential are frequently seen in electrochemical systems. Here, we adapt concepts used to understand oscillatory behavior in chemical systems of relevance to living systems to analyze the present case.[22,23]

We begin by referring to Figure 1a and Scheme 1a, which depicts the porous layer of the GDE being saturated with CO_2, leading to a steady CO_2RR at the cathode. However, possibly due to electrowetting caused by the very negative potential on the current collector (CC) of the cathode plate (CP), there is an increasing amount of liquid electrolyte ingress into the GDE (Figure 4a). K^+ ions are also transported into the GDE porous layer. The flooding probably does not occur in the hydrophobic microporous layer (MPL) but occurs in the hydrophilic mesoporous substrate (MPS) via the water path of (maybe invisible) crack regions in the MPL. (The SEM photographs of GDE with voltage oscillation and no voltage oscillation are shown in Figure S18.) Initially the diffusion of the CO_2 within the MPL layer is sufficiently fast to supply the Cu catalyst and CO_2RR is minimally affected because the gas paths remain in the MPS. At the same time, the salts of $KHCO_3$ begin to precipitate in the flow field channels (as seen by the camera) and possibly within the water-front regions of MPS in GDE (this possibility has been suggested by Moss et al.[18]) because the K^+ ions react with the supplied CO_2 gas and the salt concentration of the electrolyte reaches the precipitation concentration due to the water consumption by reductions (Figure 4b). At a certain point, CO_2 access to the Cu catalyst is abruptly stopped and the HER becomes the dominant reaction because the electrolyte flooding covers the whole MPL region and prevents most of the CO_2 supply to the Cu catalyst region, as shown in Figure 4c.

While the HER is the dominant reaction, there are concurrent phenomena that trigger the transition back to the CO_2RR. Generation of H_2 gas at the cathode and the consumption of the water will reduce the water amount in the cathode (Figure 4d). While gas is generated by the CO_2RR, the volume of gas generated by the HER is larger because of +1/2 molecules per electron for the HER and −1/12 molecules per electron for the CO_2RR to C_2H_4. The water consumptions for H_2 formation and CO_2RR to C_2H_4 are 1 and 2/3 molecule per electron, respectively (Supplementary Movie 3). Further, the liquid electrolyte in the GDE will be depleted in carbonate species since the CO_2 supply is stopped under this HER condition.[17,18] This will change the bulk pH of the cathode electrolyte from near-neutral to alkaline. (The bulk pH change model experiments changing with Ar and CO_2 supply are shown in Figure S19. The pHs at the vent of the anolyte for CO_2 reduction and H_2 formation were around 7.30 and 7.65, respectively. This supports our assertion that the local pH around the cathode catalyst increases.) Since the precipitation concentration of K_2CO_3 (the solubility in water is ca. 8.1 mol/L at 20 °C), which is the existing form in alkaline solution, is much higher than that of $KHCO_3$ (the solubility in water is ca. 3.3 mol/L at 20 °C), the liquid electrolyte accessing the cathode flow field channels is able to dissolve the salt precipitates (maybe also the salts we cannot see that are inside the GDE). These effects combine to restore, again rather abruptly, the access of CO_2 to the cathode such that the CO_2RR can restart due to the appearance of the CO_2 gas paths. The chemical reaction details are discussed in section S.4, Voltage oscillation analysis.

This pH change is also supported by the series resistance of the HER being lower than that of the CO_2RR discussed in the GEIS of Figure 3c because the resistivity of K_2CO_3 is generally lower the that of $KHCO_3$ due to their ion concentration differences.

Our model explains some observed phenomena like abrupt changes from the CO_2RR to HER and vice versa (Figure 3) and the observation of oscillations with (1) a different GDE (Figure S20), (2) use of a CO-forming Ag catalyst (Figure S21), and (3) supply of humidified CO_2 to the cell (Figure S22),[24−26] as shown in section S.6, Other supporting data for the voltage oscillation.

In summary, we conducted real-time observations of electrodes using a CMOS camera in a zero-gap type reactor with a transparent cathode end plate to understand the voltage oscillation with the transition from the CO_2RR and HER. The salt precipitation and electrolyte flooding in the cathode occurs at the CO_2RR and the amount of electrolyte decreases with the HER, respectively. From these observations, a model of the fluctuation is proposed. In this model, liquid electrolyte volume fluctuations in the cathode influence the switching between the dominant CO_2RR and HER at the cathode electrode. The change from the CO_2RR to the HER is caused by the complete electrolyte covering of the cathodic catalyst, and the opposite is caused by partial CO_2 supply recovery to the cathodic catalyst. The results show that the order of the voltage oscillation process is different from that of the previous model.[18] The effective mitigation of this voltage oscillation is thought to prevent liquid electrolyte flooding over the CO_2RR catalyst region by controlling the electrolyte migration from the anode.

https://doi.org/10.1021/acsenergylett.4c01256
ACS Energy Lett. 2024, 9, 4225−4232

■ ASSOCIATED CONTENT

Supporting Information

The Supporting Information is available free of charge at https://pubs.acs.org/doi/10.1021/acsenergylett.4c01256.

Salt precipitation and flooding on cathode (MP4)

Transition from salt precipitation to flooding on electrode and argon replacement from CO_2 gas (MP4)

Correlation between the applied voltage and flooding (MP4)

Time course of the phase portrait of partial current densities for HER and CO_2RR to ethylene (MP4)

Reactor structures and experimental conditions, supporting data for the voltage oscillation under constant current, electrolyte migration dependence on the pressure between the anode and the cathode, voltage oscillation analysis, model evaluation of the voltage oscillation analysis, other supporting data for voltage oscillation, and captions for Movies 1−4 (PDF)

■ AUTHOR INFORMATION

Corresponding Authors

Joel W. Ager, III − *Department of Materials Science and Engineering, University of California at Berkeley, Berkeley, California 94720, United States; Chemical Sciences Division, Lawrence Berkeley National Laboratory, Berkeley, California 94720, United States;* orcid.org/0000-0001-9334-9751; Email: jwager@lbl.gov

Katsushi Fujii − *Advanced Photonics Technology Development Group, RIKEN Center for Advanced Photonics, 351-0198 Saitama, Japan;* orcid.org/0000-0002-9022-9858; Email: katsushi.fujii@riken.jp

Authors

Nagisa Mikami − *Advanced Photonics Technology Development Group, RIKEN Center for Advanced Photonics, 351-0198 Saitama, Japan*

Kei Morishita − *Advanced Photonics Technology Development Group, RIKEN Center for Advanced Photonics, 351-0198 Saitama, Japan*

Takeharu Murakami − *Advanced Photonics Technology Development Group, RIKEN Center for Advanced Photonics, 351-0198 Saitama, Japan*

Takuya Hosobata − *Ultrahigh Precision Optics Technology Team, RIKEN Center for Advanced Photonics, 351-0198 Saitama, Japan*

Yutaka Yamagata − *Ultrahigh Precision Optics Technology Team, RIKEN Center for Advanced Photonics, 351-0198 Saitama, Japan*

Takayo Ogawa − *Advanced Photonics Technology Development Group, RIKEN Center for Advanced Photonics, 351-0198 Saitama, Japan*

Yoshiharu Mukouyama − *Division of Science, College of Science and Engineering, Tokyo Denki University, Hatoyama, Saitama 350-0394, Japan; Research Center for Solar Energy Chemistry, Osaka University, Toyonaka, Osaka 560-8531, Japan;* orcid.org/0000-0003-3057-2467

Shuji Nakanishi − *Research Center for Solar Energy Chemistry, Osaka University, Toyonaka, Osaka 560-8531, Japan;* orcid.org/0000-0002-3313-2689

Satoshi Wada − *Advanced Photonics Technology Development Group, RIKEN Center for Advanced Photonics, 351-0198 Saitama, Japan*

Complete contact information is available at: https://pubs.acs.org/10.1021/acsenergylett.4c01256

Author Contributions

N.M., K.M., and T.M. contributed equally to this work. N.M., T.O., S.W., and K.F. designed the research. T.H., T.M., and Y.Y. designed the transparent cell. N.M., K.M., and T.M. performed experiments and obtained data. N.M., K.M., T.M., Y.M., S.N., J.W.A., and K.F. established the reaction model. N.M., J.W.A., and K.F. wrote the paper.

Notes

The authors declare no competing financial interest.

■ ACKNOWLEDGMENTS

We thank Ms. Y, Qin for preparing the electrode and Dr. Y. Kinosita for preparing the manuscript. This research was partially based on integrated electrochemical systems for scalable CO_2 conversion to chemical feedstock projects performed as part of the Moonshot Research and Development Program funded by the New Energy and Industrial Technology Development Organization (JPNP18016). The work of J.W.A. (analysis of switching mechanism) was supported by the Clean Energy Manufacturing Program, U.S. Department of Energy, Office of Science, Office of Basic Energy Sciences, Chemical Sciences, Geosciences, and Biosciences Division, under contract no. DE-AC02-05CH11231.

■ REFERENCES

(1) Nitopi, S.; Bertheussen, E.; Scott, S. B.; Liu, X.; Engstfeld, A. K.; Horch, S.; Seger, B.; Stephens, I. E. L.; Chan, K.; Hahn, C.; Nørskov, J. K.; Jaramillo, T. F.; Chorkendorff, I. Progress and Perspectives of Electrochemical CO2 Reduction on Copper in Aqueous Electrolyte. *Chem. Rev.* **2019**, *119* (12), 7610−7672.

(2) Wakerley, D.; Lamaison, S.; Wicks, J.; Clemens, A.; Feaster, J.; Corral, D.; Jaffer, S. A.; Sarkar, A.; Fontecave, M.; Duoss, E. B.; Baker, S.; Sargent, E. H.; Jaramillo, T. F.; Hahn, C. Gas diffusion electrodes, reactor designs and key metrics of low-temperature CO2 electrolysers. *Nature Energy* **2022**, *7* (2), 130−143.

(3) Hori, Y., Electrochemical CO2 Reduction on Metal Electrodes. In *Modern Aspects of Electrochemistry*; Vayenas, C. G., White, R. E., Gamboa-Aldeco, M. E., Eds.; Springer New York: 2008; pp 89−189.

(4) Higgins, D.; Hahn, C.; Xiang, C.; Jaramillo, T. F.; Weber, A. Z. Gas-Diffusion Electrodes for Carbon Dioxide Reduction: A New Paradigm. *ACS Energy Letters* **2019**, *4* (1), 317−324.

(5) Wu, Y.; Charlesworth, L.; Maglaya, I.; Idros, M. N.; Li, M.; Burdyny, T.; Wang, G.; Rufford, T. E. Mitigating Electrolyte Flooding for Electrochemical CO2 Reduction via Infiltration of Hydrophobic Particles in a Gas Diffusion Layer. *ACS Energy Letters* **2022**, *7* (9), 2884−2892.

(6) Sander, R. Compilation of Henry's law constants (version 4.0) for water as solvent. *Atmos. Chem. Phys.* **2015**, *15* (8), 4399−4981.

(7) Tamimi, A.; Rinker, E. B.; Sandall, O. C. Diffusion Coefficients for Hydrogen Sulfide, Carbon Dioxide, and Nitrous Oxide in Water over the Temperature Range 293−368 K. *Journal of Chemical & Engineering Data* **1994**, *39* (2), 330−332.

(8) Ge, L.; Rabiee, H.; Li, M.; Subramanian, S.; Zheng, Y.; Lee, J. H.; Burdyny, T.; Wang, H. Electrochemical CO2 reduction in membrane-electrode assemblies. *Chem.* **2022**, *8* (3), 663−692.

(9) Inoue, A.; Harada, T.; Nakanishi, S.; Kamiya, K. Ultra-high-rate CO2 reduction reactions to multicarbon products with a current density of 1.7 A cm−2 in neutral electrolytes. *EES Catalysis* **2023**, *1* (1), 9−16.

(10) Kutz, R. B.; Chen, Q.; Yang, H.; Sajjad, S. D.; Liu, Z.; Masel, I. R. Sustainion Imidazolium-Functionalized Polymers for Carbon Dioxide Electrolysis. *Energy Technology* **2017**, *5* (6), 929−936.

(11) Leonard, M. E.; Clarke, L. E.; Forner-Cuenca, A.; Brown, S. M.; Brushett, F. R. Investigating Electrode Flooding in a Flowing Electrolyte, Gas-Fed Carbon Dioxide Electrolyzer. *ChemSusChem* **2020**, *13* (2), 400−411.
(12) Reyes, A.; Jansonius, R. P.; Mowbray, B. A. W.; Cao, Y.; Wheeler, D. G.; Chau, J.; Dvorak, D. J.; Berlinguette, C. P. Managing Hydration at the Cathode Enables Efficient CO2 Electrolysis at Commercially Relevant Current Densities. *ACS Energy Letters* **2020**, *5* (5), 1612−1618.
(13) Xu, Y.; Edwards, J. P.; Liu, S.; Miao, R. K.; Huang, J. E.; Gabardo, C. M.; O'Brien, C. P.; Li, J.; Sargent, E. H.; Sinton, D. Self-Cleaning CO2 Reduction Systems: Unsteady Electrochemical Forcing Enables Stability. *ACS Energy Letters* **2021**, *6* (2), 809−815.
(14) Kovalev, M. K.; Ren, H.; Zakir Muhamad, M.; Ager, J. W.; Lapkin, A. A. Minor Product Polymerization Causes Failure of High-Current CO2-to-Ethylene Electrolyzers. *ACS Energy Letters* **2022**, *7* (2), 599−601.
(15) Gabardo, C. M.; O'Brien, C. P.; Edwards, J. P.; McCallum, C.; Xu, Y.; Dinh, C.-T.; Li, J.; Sargent, E. H.; Sinton, D. Continuous Carbon Dioxide Electroreduction to Concentrated Multi-carbon Products Using a Membrane Electrode Assembly. *Joule* **2019**, *3* (11), 2777−2791.
(16) Ma, Z.; Yang, Z.; Lai, W.; Wang, Q.; Qiao, Y.; Tao, H.; Lian, C.; Liu, M.; Ma, C.; Pan, A.; Huang, H. CO2 electroreduction to multicarbon products in strongly acidic electrolyte via synergistically modulating the local microenvironment. *Nat. Commun.* **2022**, *13* (1), 7596.
(17) Garg, S.; Xu, Q.; Moss, A. B.; Mirolo, M.; Deng, W.; Chorkendorff, I.; Drnec, J.; Seger, B. How alkali cations affect salt precipitation and CO2electrolysis performance in membrane electrode assembly electrolyzers. *Energy Environ. Sci.* **2023**, *16* (4), 1631−1643.
(18) Moss, A. B.; Garg, S.; Mirolo, M.; Giron Rodriguez, C. A.; Ilvonen, R.; Chorkendorff, I.; Drnec, J.; Seger, B. In operando investigations of oscillatory water and carbonate effects in MEA-based CO2 electrolysis devices. *Joule* **2023**, *7* (2), 350−365.
(19) Na, Y.; Ha, M. G.; Park, H. S.; Park, H. Y.; Kim, H.-J.; Henkensmeier, D.; Yoo, S. J.; Kim, J. Y.; Lee, S. Y.; Jang, J. H. Effect of Dual-Flow Channel Structures on Electrochemical CO2 Reduction in Proton Exchange Membrane Electrolyzers. *Frontiers in Energy Research* **2022**, *10*, 1.
(20) Wheeler, D. G.; Mowbray, B. A. W.; Reyes, A.; Habibzadeh, F.; He, J.; Berlinguette, C. P. Quantification of water transport in a CO2 electrolyzer. *Energy Environ. Sci.* **2020**, *13* (12), 5126−5134.
(21) Luo, X.; Rojas-Carbonell, S.; Yan, Y.; Kusoglu, A. Structure-transport relationships of poly(aryl piperidinium) anion-exchange membranes: Eeffect of anions and hydration. *J. Membr. Sci.* **2020**, *598*, No. 117680.
(22) Semenov, S. N.; Kraft, L. J.; Ainla, A.; Zhao, M.; Baghbanzadeh, M.; Campbell, V. E.; Kang, K.; Fox, J. M.; Whitesides, G. M. Autocatalytic, bistable, oscillatory networks of biologically relevant organic reactions. *Nature* **2016**, *537* (7622), 656−660.
(23) Semenov, S. N.; Wong, A. S. Y.; van der Made, R. M.; Postma, S. G. J.; Groen, J.; van Roekel, H. W. H.; de Greef, T. F. A.; Huck, W. T. S. Rational design of functional and tunable oscillating enzymatic networks. *Nature Chem.* **2015**, *7* (2), 160−165.
(24) Baumgartner, L. M.; Koopman, C. I.; Forner-Cuenca, A.; Vermaas, D. A. When Flooding Is Not Catastrophic—Woven Gas Diffusion Electrodes Enable Stable CO2 Electrolysis. *ACS Applied Energy Materials* **2022**, *5* (12), 15125−15135.
(25) Edwards, J. P.; Alerte, T.; O'Brien, C. P.; Gabardo, C. M.; Liu, S.; Wicks, J.; Gaona, A.; Abed, J.; Xiao, Y. C.; Young, D.; Sedighian Rasouli, A.; Sarkar, A.; Jaffer, S. A.; MacLean, H. L.; Sargent, E. H.; Sinton, D. Pilot-Scale CO2 Electrolysis Enables a Semi-empirical Electrolyzer Model. *ACS Energy Letters* **2023**, *8* (6), 2576−2584.
(26) Hoof, L.; Thissen, N.; Pellumbi, K.; junge Puring, K.; Siegmund, D.; Mechler, A. K.; Apfel, U.-P. Hidden parameters for electrochemical carbon dioxide reduction in zero-gap electrolyzers. *Cell Reports Physical Science* **2022**, *3* (4), No. 100825.

https://doi.org/10.1021/acsenergylett.4c01256
ACS Energy Lett. 2024, 9, 4225−4232